Published in final edited form as:
J Control Release. 2013 May 28; 168(1): 41–49. doi:10.1016/j.jconrel.2013.02.004.

Optimization of cell receptor-specific targeting through multivalent surface decoration of polymeric nanocarriers

Suzanne M. D'Addio[1], **Steven Baldassano**[1], **Lei Shi**[1], **Lila Cheung**[1], **Douglas H. Adamson**[1], **Matthew Bruzek**[2], **John E. Anthony**[2], **Debra L. Laskin**[3], **Patrick J. Sinko**[3], and **Robert K. Prud'homme**[1,*]

[1]Chemical and Biological Engineering, Princeton University, Princeton, NJ 08544

[2]Department of Chemistry, University of Kentucky, Lexington, KY, 40506

[3]Ernest Mario School of Pharmacy, Rutgers University, Piscataway, NJ, 08854

Abstract

Treatment of tuberculosis is impaired by poor drug bioavailability, systemic side effects, patient non-compliance, and pathogen resistance to existing therapies. The mannose receptor (MR) is known to be involved in the recognition and internalization of *Mycobacterium tuberculosis*. We present a new assembly process to produce nanocarriers with variable surface densities of mannose targeting ligands in a single step, using kinetically-controlled, block copolymer-directed assembly. Nanocarrier association with murine macrophage J774 cells expressing the MR is examined as a function of incubation time and temperature, nanocarrier size, dose, and PEG corona properties. Amphiphilic diblock copolymers are prepared with terminal hydroxyl, methoxy, or mannoside functionality and incorporated into nanocarrier formulations at specific ratios by Flash NanoPrecipitation. Association of nanocarriers protected by a hydroxyl-terminated PEG corona with J774 cells is size dependent, while nanocarriers with methoxy-terminated PEG coronas do not associate with cells, regardless of size. Specific targeting of the MR is investigated using nanocarriers having 0-75% mannoside-terminated PEG chains in the PEG corona. This is a wider range of mannose densities than has been previously studied. Maximum nanocarrier association is attained with 9% mannoside-terminated PEG chains, increasing uptake more than 3-fold compared to non-targeted nanocarriers with a 5 kg mol^{-1} methoxy-terminated PEG corona. While a 5 kg mol^{-1} methoxy-terminated PEG corona prevents non-specific uptake, a 1.8 kg mol^{-1} methoxy-terminated PEG corona does not sufficiently protect the nanocarriers from nonspecific association. There is continuous uptake of MR-targeted nanocarriers at 37°C, but a saturation of association at 4°C. The majority of targeted nanocarriers associate with J774E cells are internalized at 37°C and uptake is receptor-dependent, diminishing with competitive inhibition by dextran. This characterization of nanocarrier uptake and targeting provides promise for optimizing drug delivery to macrophages for TB treatment and establishes a general route for optimizing targeted formulations of nanocarriers for specific delivery at targeted sites.

*Author for Correspondence, Department of Chemical and Biological Engineering, Princeton University, Princeton, NJ 08854 USA Tel: (609) 258-4577 Fax: (609) 258-0211, prudhomm@princeton.edu.

Supplementary data. Further details on synthesis, ^{1}H NMR, FPN, and NC association experiments are available in the Supplementary Information, which can be found online at http://.

1. Introduction

Tuberculosis (TB) is an intracellular infection which affects 1 in 3 people worldwide and causes over 1 million deaths yearly [1]. During TB infection, *Mycobacterium tuberculosis* (*M. tuberculosis)* bacilli are phagocytized by host immune cells and the normal enzymatic digestion process is arrested [2], which allows the bacteria to replicate within the host cells [3]. Treatment of the infection is hindered by poor drug permeability, solubility, or biodegradation [4, 5] and the increasing threat of multiple drug resistant TB (MDR-TB) has led to a search for improved therapeutics [1]. One approach has been to improve drug localization at the infection site through active targeting with ligands specific for the diseased tissue [6]. In TB infection, the pattern-recognition mannose receptor (MR) binds to mannose caps on the *M. tuberculosis* coat protein, lipoarabinomannan, and also mediates phagocytosis [2, 7]. Therefore, designing nanocarriers (NCs) which target drug payloads to cells expressing MR can improve the co-localization of anti-TB drugs with infected cells.

MR-targeted liposomal systems have been studied as therapeutics [8-10] and adjuvants [11]. While liposomes are effective for the delivery of hydrophilic therapeutics, their small hydrophobic volumes make them ineffective for the delivery of hydrophobic actives. Polymeric NCs composed of a drug core stabilized by amphiphilic diblock copolymers can be formed at high drug loadings by Flash NanoPrecipitation (FNP) [12] and are effective candidates for formulating novel hydrophobic TB therapeutics [13, 14]. In addition, targeting functionality can be incorporated into the stabilizing block copolymers [15, 16]. The success of a targeted formulation is dependent on targeting a pathway specific to the disease pathology. Macrophages, dendritic cells, and other cells of the immune system specifically express surface carbohydrate binding proteins, referred to as lectins, which are involved in the phagocytosis of several intracellular pathogens, including *M. tuberculosis* [17]. Classes of lectins recognize common motifs, but ligand specificity between different receptors is determined by the orientation of the carbohydrate binding domain. The MR, which belongs to this class of surface receptors, is a macrophage transmembrane protein possessing multiple carbohydrate binding sites. Binding of terminal mannose and fucose moieties is favored by the MR and the sugar density on ligands is crucial for high affinity binding [18, 19], but receptor oligomerization is not required for internalization [19, 20]. Since *M. tuberculosis* uptake is mediated by the MR, we target antitubercular drugs to the MR *via* terminal mannoside moieties on NC surfaces, in a way that mimics lipoarabinomannan coating of TB bacilli.

Studies have been published that demonstrate improved uptake of various mannosylated NCs relative to non-targeted formulations, including liposomes [8, 11, 21, 22], gelatin nanoparticles [23], and oil in water emulsions [24]. The binding and internalization of NCs by a MR mediated pathway is influenced by the relative ligand surface density [8, 9, 24, 25] and the length of the PEG spacer between mannoside and the particle surface [26]. Prior reports for liposomes indicate increasing cellular association with increasing mannoside surface density, but the surface densities explored in these studies were limited to 30 and 60% [8], or 2.5%, 5%, and 7.5% [9, 24]. The phagocytosis of PEGylated 5 μm microspheres by macrophages *in vitro* was increased only at 34 and 45% mannosylated PEG chains, relative to 100% methoxy-terminated PEG chains, which were the highest compositions tested [25]. In these reports, the number of mannose moieties is not reported, and so a direct comparison of the ligand surface density cannot be made. There have not been reports of a polymeric NC system in which surface mannosylation is controlled to find the optimal NC composition to maximize cellular association *via* the MR. Recent studies have systematically explored the importance of ligand surface density on NC association with cell surface receptors, and results indicate that binding and uptake do not increase monotonically with increasing surface ligand density. It has been found that there exists an optimum

surface density for binding and uptake of NCs which have been modified with peptide [27] and folate [28-30] targeting ligands.

In this work, we formulate and characterize MR targeted NCs in order to optimize association with macrophages expressing the MR. PEGylated NCs with 7 different ligand surface densities and 2 different methoxy-terminated PEG molecular weights are prepared by rapid precipitation and directed assembly of amphiphilic diblock copolymers in FNP. The FNP process enables the assembly of functional NCs with variable surface properties in a quantitative and efficient manner. The association with macrophages *in vitro* is then characterized as a function of incubation time and temperature, NC size, dose dependence, and polymer structure. In these experiments we use the murine macrophage J774 cell line, which was chosen since it has been extensively studied [31-33], multiple clones have been isolated [34] with quantified mannose receptor expression [33], and it has been used in previous studies of NC uptake [23, 35-38]. We obtain two J774 clones: the J774E clone which over-expresses the mannose receptor (98,200 binding sites per cell in suspension), and the J774A.1 clone which has approximately half the number of receptors [33]. The J774A.1 clone has been previously used to study nanocarrier interactions with cells *in vitro* and for *in vitro* TB models, and we find the cellular association of PEG protected NCs with a single methoxy or hydroxyl terminal group on PEG demonstrates an unexpected sensitivity to the terminal group and NC size. With the J774E clone, we show that targeting the MR triples NC uptake relative to the methoxy-terminated PEGylated NCs. We present the first results indicating that uptake of mannoside functionalized NCs by macrophages does not saturate with increasing mannose functionalization, but has a relatively sharp maximum. These findings have significant implications for enhanced localization of therapeutic TB drugs.

2. Materials and methods

2.1. Materials

Tetrahydrofuran (THF, 99.9%), dichloromethane (DCM, 99.5%), dimethylsulfoxide (DMSO), hexane, ethyl acetate, anhydrous ethyl ether (ether) and sodium bicarbonate were purchased through Fisher Scientific (Pittsburgh, PA). Vitamin E (VE, 97%) and dextran (M_w = 60-80 kg mol^{-1}) were purchased from Sigma-Aldrich (St. Louis, MO). Anhydrous magnesium sulfate ($MgSO_4$) was from EMD Chemicals INC (Gibbstown, NJ). Prior to use, water was purified by 0.2 μm filtration and four stage deionization to a resistivity of 17.8 MΩ or greater (NANOpure Diamond, Barnstead International. Dubuque, IA). The block copolymers are designated:"XXX_m-PEG_n-**YY**", where XXX designates the hydrophobic block type, m is the M_w of the hydrophobic block in g mol^{-1}, n is the M_w of the PEG block in g mol^{-1}, and **YY** is the terminal group on PEG (methoxy: **OCH_3**, hydroxyl: **OH**, mannoside: **MAN**). Poly-D,L-lactide-*b*-polyethylene glycol ($PLA_{3.8k}$-*b*-PEG_{5k}-**OCH_3**) was kindly provided by Evonik, Inc. (Birmingham, AL). $PS_{1.6k}$-*b*-$PEG_{1.8k}$-**OH** was purchased from Polymer Source (Dorval, QC, CAN) and the synthesis of $PS_{1.5k}$-*b*-PEG_{5k}-**OH** has been reported previously [39]. For the latter polymer, prior to polymerization of PEG, a fraction of the $PS_{1.5k}$-OH was set aside and used as a hydrophobic filler in the NC formulations. J774A.1 murine macrophages were obtained from the American Type Culture Collection (ATCC. Manassas, VA); J774E cells were provided by Dr. Philip Stahl (Washington University. St. Louis, MO). Dulbecco's modified Eagle medium (high-glucose with sodium pyruvate and L-glutamine), fetal bovine serum (FBS), and penicillin-streptomycin (Penicillin-5,000 IU mL^{-1}, Streptomycin-5 mg mL^{-1}) were from Fisher Scientific.

2.2. Conjugation to form $PS_{1.5k}$-b-PEG_{5k}-MAN (5) [40]

The syntheses of precursor compounds **1**-**4** and the TBTA catalyst are detailed in the Supplemental Information (SI). **3** (0.138 g) and **4** (0.5 g) were dissolved in 26 mL of degassed anhydrous THF. TBTA (0.0035 g) and CuBr (catalytic, Alfa Aesar. Ward Hill, MA) were dissolved in 15 mL of dry THF and transferred to the solution of **3** and **4**. The reaction was stirred for 2 days and was then dialyzed (regenerated cellulose, MWCO: 3.5 kD, Spectra/Por) against THF (350 mL × 3) for 1 d followed by dialysis in DI H_2O (2 L × 4) for 2.5 d. The product was dried by lyophilization and 0.13 g was recovered (Yield: 24 %).

2.3. Synthesis of PS_m-b-PEG_n-OCH_3 (6)

This procedure was based on Aoyama *et al.* [41], and details on the adaptation are available in the SI. PS_m-*b*-PEG_n-**OH** (0.147mmol, $PS_{1.5k}$-*b*-PEG_{5k}-**OH** or $PS_{1.6k}$-*b*-$PEG_{1.8k}$-**OH**) was dissolved in 19.75 mL DCM and cooled in an ice bath. After adding aqueous trifluoroboric acid (0.025 mL, 48%, Alfa Aesar), 0.88 mL of trimethyl silyldiazomethane (2M in Hexane, $TMSCHN_2$, Alfa Aesar) was added dropwise over 4 min. In subsequent 20 min intervals, 0.44 mL, 0.22 mL, and 0.22 mL of $TMSCHN_2$ were added and gas was evolved. The mixture was stirred overnight at 4°C. The reaction solution was extracted once with 20 mL brine, the organic phase was dried over $MgSO_4$ and concentrated to 3 mL. The polymer was precipitated in ether, chilled by dry ice, and isolated by centrifugation (15 min, 1000 × g, 4°C). The end group conversion was determined by NMR analysis (see SI, S.3.3).

2.4. Nanocarrier formulation

A multi inlet vortex mixer (MIVM) geometry [12, 42] was used to prepare Formulation 1.1 (Table 1) at high supersaturation with mixing times on the order of 1.5 ms (SI, Fig. S.6a). In this mixing scheme, a THF stream containing a solution of $PS_{1.5k}$-OH (7.5 mg mL^{-1}), EtTP5 (2.5 mg mL^{-1}), and $PS_{1.5k}$-*b*-PEG_{5k}-**OH** (10 mg mL^{-1}), was fed into the MIVM by a digitally controlled syringe pump (Harvard Apparatus, PHD 2000 programmable, Holliston, MA) at 12 mL min^{-1}, and was mixed against 3 streams of water at a combined flow rate of 108 mL min^{-1}.

Small scale (10 mL) NC formulations with variable sizes or mannose surface densities were prepared using a confined impinging jets (CIJ) mixer (SI, Fig. S.6b) which has been shown to have robust mixing while enabling formulation on a smaller scale than in the MIVM [43]. Formulations 1.2-1.7 in Table 1 and formulations 2.1-2.14 in Table 2 were prepared using the CIJ mixer. A 1 mL THF solution with the dissolved NC components, detailed in Tables 1 and 2, was loaded into a plastic syringe (5 mL Norm-Ject®) and mixed against 1 mL of DI water. Both syringes were driven manually, and the mixed stream was collected in 8 mL of stirred water. The syringes were emptied at the same rate and in less than 2 s to produce a mixing Reynolds number of Re~1300 [12].

NC size in Formulations 1.2-1.7 (Table 1) was controlled by the amount of the filler used. Particle sizes from 62 nm to 204 nm, with various surface functionalities were prepared. EtTP5 was included in all formulations to facilitate quantitation of the NCs by a florescence assay. EtTP5 is a hydrophobic fluorescent compound originally developed for use in organic light emitting diodes, and designed to minimize aggregation-induced quenching [44]. In Table 2, the ratio of stabilizing polymers was set to control the percent of mannosylated surface chains, and the total number of moles of stabilizer was constant at 1.5×10^{-6} mol mL^{-1}.

After FNP, THF was removed from the NC suspensions by dialysis using a Spectra/Por® regenerated cellulose dialysis membrane with a molecular weight cut off (MWCO) of 6-8 kD against 1 L of water at room temperature, which was refreshed 4 times over 24 hours.

Dynamic light scattering (DLS) was used to determine the intensity weighted particle size distribution (PSD) and intensity average particle diameter for each NC suspension. Each NC suspension was diluted in water until translucent and the size was measured using a ZetaSizer Nano ZS (Malvern Instruments. Worcestershire, U.K.).

2.5. Cell culture experiments

J774A.1 and J774E mouse macrophages were cultured in DMEM, supplemented with 3.6 g L^{-1} sodium bicarbonate, 10% FBS, penicillin (50 IU mL^{-1}) and streptomycin (50 μg mL^{-1}) (hereafter referred to as 1X Media), at 37°C and 5% CO_2. For experiments, 2X Media was prepared (1 g of powdered DMEM, 3.6 g sodium bicarbonate and 500 mL water), sterile filtered, and supplemented with 20% FBS. For NC association experiments, J774A.1 and J774E cells were inoculated into 24 well dishes (8×10^5 cells mL^{-1} $well^{-1}$). After 24 h incubation, the media containing unattached cells was removed, and the cells were re-fed with culture media containing NC suspensions. Media for experiments was prepared by mixing equal volumes of aqueous NC suspensions and 2X Media, followed by further dilution with 1X Media, to achieve the target concentrations of NCs. The concentration of NC core material, c_{core}, is the sum of EtTP5 dye concentration, c_{EtTP5}, and filler, c_{filler} (where the filler is VE or $PS_{1.5k}$-OH), and c_{core}= 100 μg mL^{-1} in all trials, unless stated otherwise. All *in vitro* experiments were carried out with 10% FBS.

2.6. Quantifying NC uptake

Uptake of NC was quantified by solubilizing the hydrophobic dye encapsulated in the NC core to extract it from the lysed cell debris. The dissolved dye was then quantified by fluorescence spectroscopy. After incubating the cells with the NCs, the media was removed and the cells washed 3X with HBSS to remove unassociated NCs. The cells were then lysed in 1 mL of 0.1% (w/v) Triton X-100 (Sigma Aldrich) for 45 min in the dark. The lysates were frozen in 2 mL microcentrifuge tubes (Fisher) on dry ice prior to lyophilization in a VirTis AdVantage 2.0 BenchTop Freeze Dryer (Gardiner, NY) for 24 h at room temperature and < 30 mtorr. THF was added to the dried powders to dissolve the NCs which had associated with the cells. The mixture was centrifuged at 7000×g for 10 min to settle the insoluble cellular material. The fluorescence of the transparent supernatant was measured using a Hitachi F-7000 Fluorescence Spectrophotometer (Hitachi High-Technologies Corporation), with an excitation wavelength of 485 nm. The peak value in the fluorescence emission spectrum at 632 nm was used to quantify the EtTP5 mass associated with cells in each well, m_{EtTP5}, using a fluorescence correlation. Control wells incubated without NCs had baseline fluorescence values. Using the measured value for m_{EtTP5} for each sample, the total NC core mass associated with the cells, m_{core}, was calculated from the ratio of concentrations of EtTP5, to total core mass in the NC, based on Table 1 and 2: $(m_{EtTP5}/m_{core})=(c_{EtTP5}/c_{EtTP5}+c_{filler})$. The mass of the core associated with the cells, m_{core}, was normalized by area of the confluent cell monolayer.

2.7. Confocal imaging

Cells were plated onto 4 chamber glass slides (2.5×10^5 cells mL^{-1} in 0.5 mL 1X Media). After 24 h incubation, the media was replaced with NC dilutions in 1X media, prepared as described above, After various incubation times, the media was removed, the cells washed 3X with HBSS and fixed in 0.5 mL of 3.7% paraformaldehyde in PBS. After 1 h, the slides were rinsed with PBS, stained with DAPI in McIlvains Buffer (0.1 M citric acid, 0.2 M Na_2HPO_4, pH = 7), and rinsed again with PBS. Cells were then examined using a Leica TCS SP5 with a HCX PL APO 63.0x1.30 glycerin objective lens at 60X magnification. DAPI stain was imaged by excitation with 405 nm diode laser and an emission band from 401-443 nm. The EtTP5 fluorescent dye in the core of the NCs was excited with an argon lamp and the emission from 600-725 nm was collected.

3. Results

3.1. Nanocarrier association dependence on time, temperature, and dose

NCs with average diameters of 115 nm stabilized by $PS_{1.5k}$-*b*-PEG_{5k}-**OH** block copolymers (Formulation 1.1, Fig. 2 inset) were used to determine the time profiles for NC association with J774A.1 and J774E cells at 37°C and 4°C, to evaluate the kinetics of association, and the effects of NC dose. The results are reported in the SI (Section S.5, Figs. S.7-S.8).

3.2. Nanocarrier association dependence on size and terminal PEG group

$PS_{1.5k}$-PEG_{5k}-**OH** and $PLA_{3.8k}$-*b*-PEG_{5k}-$\mathbf{OCH_3}$ were used as stabilizing polymers in Formulations 1.2-1.4 and 1.5-1.7, to assess the importance of methoxy versus hydroxyl termination of the PEG. Hubbell, *et al.*, reported that 25 nm microgel particles accumulate in dendritic cells with hydroxyl-terminated PEG layers, but not those with methoxy-terminated PEG [45]. Although the chemistry and structure of these particles are very different from those presented here, the dependence on PEG termination is similar. The particle size distributions, measured by DLS, for NCs stabilized by $PS_{1.5k}$-*b*-PEG_{5k}-**OH** and $PLA_{3.8k}$-*b*-PEG_{5k}-$\mathbf{OCH_3}$ are plotted in Fig. 1a and 1b, which show monomodal and narrow particle size distributions. Increasing the ratio of core to stabilizer resulted in increased average particle diameter, as tabulated in Table 1.

Cell association experiments with these six NC formulations were performed with J774A.1 cells at 4°C for 2 h at a NC concentration of 50 $\mu g\ mL^{-1}$. The NC mass associated with the cells after the incubation period is plotted for each formulation in Fig. 1c. Low levels of association were observed for all of the NCs with methoxy-terminated PEG chains, as shown for all formulations stabilized by $PLA_{3.8k}$-*b*-PEG_{5k}-$\mathbf{OCH_3}$. The methoxy terminal group creates "stealth" NCs. In contrast, association of NCs stabilized by $PS_{1.5k}$-*b*-PEG_{5k}-**OH** increases with NC size. In this experiment, the 0.053±0.0093 $\mu g\ cm^{-2}$ association of the 105 nm NCs (Formulation 1.3) with a core of VE, at a dose of 50 $\mu g\ mL^{-1}$ (Fig. 1c) is not statistically different (p=0.2) from the 0.031±0.0023 $\mu g\ cm^{-2}$ association which was found for 115 nm NCs (Formulation 1.1) with a core of $PS_{1.5k}$-OH at a dose of 62 $\mu g\ mL^{-1}$ at 4°C (SI, Fig. S.7). Both formulations are stabilized by $PS_{1.5k}$-*b*-PEG_{5k}-**OH**, indicating that the particle size and particle surface determine the extent of association. Our earlier studies have shown that the $PS_{1.5k}$-*b*-PEG_{5k}-**OH** chains are densely packed, with a surface density of ~2 nm^2 per chain [46]; therefore, the core is sufficiently shielded by the PEG layer and is not a significant factor in the binding/uptake results.

3.3. Mannose targeting for uptake by macrophages

Since there was no significant association for $PLA_{3.8k}$-*b*-PEG_{5k}-$\mathbf{OCH_3}$ stabilized particles (Fig. 1c), methoxy-terminated polymers were synthesized for the "non-functional" polymer in targeted NC formulations. Beginning with $PS_{1.5k}$-*b*-PEG_{5k}-**OH**, the terminal hydroxyl group was modified to either -**MAN** or -$\mathbf{OCH_3}$ according to Scheme S.1 in the SI. A series of NC formulations were then produced with varying mannoside surface density by changing the relative amounts of $PS_{1.5k}$-*b*-PEG_{5k}-**MAN** and PS_m-*b*-PEG_n-$\mathbf{OCH_3}$ polymers in the NC formulation (Table 2). Formulations 2.1-2.7 in Table 2 are made with $PS_{1.5k}$-*b*-PEG_{5k}-$\mathbf{OCH_3}$ and $PS_{1.5k}$-*b*-PEG_{5k}-**MAN** so that the corona of each particle is composed of PEG chains of equal length (5 $kg\ mol^{-1}$) but with varying numbers of mannose-terminated PEG (Fig. 2a). In contrast, NC formulations 2.8-2.14 are made with $PS_{1.6k}$-*b*-$PEG_{1.8k}$-$\mathbf{OCH_3}$ and $PS_{1.5k}$-*b*-PEG_{5k}-**MAN** as the stabilizing polymers, such that the steric PEG corona is composed of short methoxy-terminated PEG chains (1.8 $kg\ mol^{-1}$),whereas the targeting mannose groups are presented on longer (5 $kg\ mol^{-1}$) PEG chains. (Fig. 2b). The goal was to see if presentation of the targeting group beyond the brush layer of the methoxy

stabilizing PEG polymer layer would enhance uptake. Within each series, the total number of moles of polymer is held constant.

The extent of NC association with J774E cells at 37°C, in the presence of serum, after 4 h, as a function of the fraction of $PS_{1.5k}$-*b*-PEG_{5k}-**MAN** in the formulation is shown in Fig. 2. When the corona was composed of all PEG_{5k}, there was a monotonic, 3.2-fold increase in NC association as the percentage of mannose conjugated chains increased from 0 to 9%. Beyond this, the amount of NC association decreases. The data at 0% mannose represents the purely sterically stabilized NCs. For non-targeted NCs with only methoxy-terminated PEG steric layers, the higher molecular weight 5 kg mol^{-1} PEG-$\mathbf{OCH_3}$ chains were more effective at inhibiting uptake than the 1.8 kg mol^{-1} PEG-$\mathbf{OCH_3}$. When the stabilizing PEG layer was 100% $PS_{1.6k}$-*b*-$PEG_{1.8k}$-$\mathbf{OCH_3}$, there was a 2.4-fold increase in NC association relative to particles with a $PS_{1.5k}$-*b*-PEG_{5k}-$\mathbf{OCH_3}$ corona. This is consistent with previous studies that have shown that 5 kg mol^{-1} PEG chains are superior to 2 kg mol^{-1} chains in sterically protecting stealth liposomes [47, 48]. At 4% and greater, the association for NCs stabilized by $PS_{1.5k}$-*b*-PEG_{5k}-$\mathbf{OCH_3}$ or $PS_{1.6k}$-*b*-$PEG_{1.8k}$-$\mathbf{OCH_3}$ is indistinguishable. Presumably the mannose ligands dominate the targeting response both in increasing and then blocking uptake.

Formulation 2.4 had the optimal mannose surface density at 9% $PS_{1.5k}$-*b*-PEG_{5k}-**MAN**, with $PS_{1.5k}$-*b*-PEG_{5k}-$\mathbf{OCH_3}$ as the stabilizing non-functional polymer. The association of this formulation was measured as a function of time at both 37°C and 4°C with J774E cells and was quantified by lysing the cells and solubilizing the dye (Fig. 3a). In addition to washing and lysing cells for quantification of NC association, cell samples on glass slides were fixed at each time point and prepared for confocal imaging (Fig. 3b-d). The quantitative results in Fig. 3a are in agreement with the results for Formulation 1.1 in SI Fig. S.8, where cells exposed to NCs at 4°C reach a relatively low, steady state amount of association, while association continues to increase with time in the cells incubated at 37°C. Confocal imaging of cells incubated with NCs at 4°C shows very little EtTP5 fluorescence, and no fluorescence in the cytosol, after 3 h of incubation with the NCs (Fig. 3c), similar to control cells which were not incubated with NCs (Fig. 3b). In contrast, the cells fluoresce strongly after incubation at 37°C for 3h in Fig. 3d, which is a representative z-slice through the middle of cells fixed at this condition. This image also shows the localization of NCs. The distribution of fluorescence in the cells is varied, with concentrated regions of fluorescence larger than 1 μm as well as pixel sized spots distributed throughout the cells. The NCs may be localized in organelles after internalization. NCs are not seen to penetrate the cell nuclei.

3.4. Inhibition of mannose receptor

To determine if internalization of mannose-targeted NCs was specifically mediated by the mannose receptor, uptake experiments in the presence of a competitive inhibitor were carried out. The MR has a higher affinity for polysaccharides than free monosaccharides due to the multiplicity of binding sites, and binding of dextran and mannan have been established [19, 49]. For inhibition experiments, J774E cells were pre-incubated at 37°C with 1 mg mL^{-1} dextran (M_w=60–80 kg mol^{-1}) for 45 min before the addition of NCs stabilized by 9% $PS_{1.5k}$-*b*-PEG_{5k}-**MAN**, $PS_{1.5k}$-*b*-PEG_{5k}-**OH**, or $PS_{1.5k}$-*b*-PEG_{5k}-$\mathbf{OCH_3}$ (Formulations 2.4, 1.1, and 2.1, respectively) suspended in media with 1 mg mL^{-1} dextran. The same NC formulations without dextran were incubated with cells that were not pre-treated with dextran. The experiment duration was 4 h at 37°C. The presence of dextran resulted in a 59% decrease (p=0.02) in the association of the optimal MR-targeted formulation in J774E cells (Formulation 2.4) (Fig. 4). In contrast, addition of dextran did not significantly affect uptake of NCs stabilized by $PS_{1.5k}$-*b*-PEG_{5k}-**OH**. Low uptake levels of $PS_{1.5k}$-*b*-PEG_{5k}-$\mathbf{OCH_3}$ stabilized NCs were consistently observed.

4. Discussion

The macrophage MR is responsible for receptor-mediated endocytosis and phagocytosis, and is specific to macrophages and macrophage-like cells [18]. Targeting the mannose receptor is appropriate for treatment of TB since *M. tuberculosis* entry to macrophages is achieved *via* MR-mediated phagocytosis. It is therefore more likely that intracellular co-localization of the bacteria and the NCs will occur. The primary goal of this research was to explore formulation of drug NCs by FNP and optimize internalization by cells *via* a specific MR-mediated pathwayAdherent cells were incubated with NCs, then washed and lysed so that the total mass associated with the cells could be quantified using extraction of the hydrophobic EtTP5 fluorophore and independent fluorescence analysis. The known mass ratio of fluorophore to total NC was used to calculate total core uptake according to the equation in Section 2.6. The total core uptake is reported since this corresponds to the drug payload that would be delivered for a therapeutic NC. NC association refers to both surface binding and internalization.

4.1 Nanocarrier association

NCs were incubated with a monolayer of either J774A.1 or J774E cells at 4°C and 37°C to assess the extent of surface association versus internalization and the effect of NC dose. The association kinetics and dose dependence are presented in SI Section S.5. The J774A.1 cells are used to investigate the size dependence of NC association [37], while targeting of the MR by NCs is conducted using the J774E cells, which over express the MR [38]. At 4°C, there was an insignificant difference in the amount of association of PEG_{5k}-**OH** coated NCs (Formulation 1.1), which reached 0.90±0.01 μg cm^{-2} on J774A.1 cells in 1 h, and 0.95±0.01 μg cm^{-2} in 1 h with J774E cells (SI, Fig. S.7). After a 4 h exposure with J774E at 4°C, the association of the same NC formulation was independent of dose above 90 μg mL^{-1} (SI, Fig. S.8) and the limit of 0.09±0.02 μg cm^{-2} corresponded to those in SI Fig. S.7. In both of these experiments, surface adsorption equilibrates, but only corresponds to 6% surface coverage (approximating the macrophage to be a dome with a height of 6 μm and a diameter of 25 μm). Therefore, the equilibrium value of NC association at 4°C does not correspond to total surface coverage. In contrast to the binding equilibrium at 4°C, cellular association increases monotonically with time at 37°C (SI, Fig. S.7) and in a dose dependent manner (SI, Fig. S.8). Confocal images of J774E cells confirmed that polymeric NCs formed by FNP are internalized by the macrophages at 37°C and confirm low levels of association at 4°C where no internalization was observed (Fig. 3c, d). Taken together, these results confirm that surface binding is thermodynamically limited at 4°C and that NCs are kinetically internalized at 37°C.

In many targeting studies reported in the literature, PEGylated nanocarriers without targeting ligands are used as a negative control to gage the contribution of the targeting ligands on binding and internalization. The terminal group on PEG depends on the synthesis route employed to form the polymer. We find that the terminal group on PEG chains plays an important role in determining the interaction with a cell monolayer. There is minimal association when a methoxy-terminated PEG chain stabilizes the particles, regardless of particle size, while there is a size dependence for NC association when PEG is terminated by a hydroxyl group (Fig. 1c). The low level of association in Fig. 2 for Formulation 2.6, which is stabilized by $PS_{1.5k}$-*b*-PEG_{5k}-$\mathbf{OCH_3}$, confirms that it is the terminal methoxy group on PEG which reduces the interaction with macrophages relative to the $PS_{1.5k}$-*b*-PEG_{5k}-**OH** (Fig. 1c), and not the particular hydrophobic block type. Hubbell observed a similar size effect for NCs stabilized by Pluronic® F127, which has two terminal PEG chains with hydroxyl end groups on each triblock chain, where 25 nm NCs were not taken up by adherent J774A.1 cells, but 100 nm NCs were [37]. The implications of this result are

important in proceeding with developing targeted nanocarrier formulations. The low, size-independent association of NCs stabilized by PEG_{5k}-**OCH_3** reveals that the surface is passivated, while the size dependent association of PEG_{5k}-**OH** stabilized NCs are not and thus not appropriate for isolating the effects of ligand surface density on binding.

Two main conclusions come from the $PS_{1.5k}$-*b*-PEG_{5k}-**OH** stabilized nanoparticle uptake result: 1) The hydroxyl terminus is required for binding to the surface and internalization by a non-MR specific uptake mechanism, and 2) Larger particles have an higher capacity for binding multiple receptors since they present a larger contact area between the NC surface and the macrophage surface. The first point has been previously reported by Hubbell [45], who showed that there is uptake of PEG-**OH** microgel particles which is suppressed when the terminal groups were PEG-**OCH_3**. The second point can be made by calculating the contact area between spheres with diameters of 60, 100, or 200 nm and a planar surface, representing the large macrophage cell surface, at a separation distance of 5.3 nm, which corresponds to the radius of gyration of a 5 kg mol^{-1} PEG chain (Fig. 5). The contact area, *A*, is calculated by determining the chord length, c_i, for each sphere in contact with the planar surface, assuming complete compression or displacement of the PEG brush at the point of contact. This contact area increases proportionately to the measured NC association with the cells at 4°C. Since the size dependence of NC binding to a cell surface emerges from the increased contact area, the PEG_{5k}-**OH** brush layer is not an appropriate passivating surface for specific targeting studies..

4.2. Nanocarrier targeting and optimized binding and uptake to the mannose receptor

The optimization of NCs for targeting is addressed in Figs. 2-4. At 0% mannose functionalization (Fig. 2, Formulation 2.1 in Table 2) we find that the $PS_{1.5k}$-*b*-PEG_{5k}-**OCH_3** stabilizer with a 5 kg mol^{-1} PEG-**OCH_3** corona minimizes association with the cell surface. The 1.6 kg mol^{-1} PEG-**OCH_3** corona formed by $PS_{1.6k}$-*b*-$PEG_{1.8k}$-**OCH_3** (Formulation 2.7 in Table 2) is only half as effective at minimizing association, where the association values are 0.16 μg/cm^2 and 0.07 μg/cm^2 for the 1.8 kg mol^{-1} versus 5 kg mol^{-1}, respectively. As was noted earlier, this is consistent with data for liposomes and for our NCs [46], where 5 kg mol^{-1} PEG provides better protection from clearance than does 2 kg mol^{-1} PEG. The most significant finding is that there is a sharp optimum in mannose density for maximum targeting. For the $PS_{1.5k}$-*b*-PEG_{5k}-**OCH_3** stabilized NCs, cellular association increases with increasing content of $PS_{1.5k}$-*b*-PEG_{5k}-**MAN** from 0 to 9%, due to improved binding by multivalent interactions with surface mannose receptors. The sharp increase in uptake at this mannose surface density indicates that there is an ideal targeting structure for binding to the macrophage mannose receptor, which shifts binding equilibrium to maximize the fraction of NCs bound to the cell surface and eligible for uptake. Additionally, the macrophage mannose receptor internalizes ligands most effectively with multivalent binding since high affinity binding and uptake requires participation of more than one of the receptor's eight carbohydrate binding locations [49]. However, mannose surface density greater than 9% is detrimental to uptake. The exact cause is unclear at this time, but it is possible that binding of too many receptors results in overstimulation of the intracellular signal pathways mediating endocytosis or increases membrane rigidity due to multivalent receptor aggregation [45]. The result shows that rather than an increase in binding and saturation, there is an optimum. As was noted, similar optimum values in ligand density for targeting have been observed for folate targeting. The ease with which FNP can create a library of NCs with varying ligand density, by merely controlling the relative concentrations of polymers in the FNP assembly process, is a major advantage of this technique. It enables preparation of samples to address fundamental questions in targeting and delivery.

The second major finding for the design of targeted NCs concerns the presentation of the targeting ligand relative to the steric stabilizing PEG layer. It was hypothesized that the greater polymer flexibility and mannose availability for $PS_{1.5k}$-*b*-PEG_{5k}-**MAN** chains which extend beyond the $PS_{1.6k}$-*b*-$PEG_{1.8k}$-$\mathbf{OCH_3}$ corona would enable greater targeting efficiency. The relatively small mannose might have been less available for binding if it is buried in the 5 kg mol^{-1} PEG corona with all of the PEG chains being 5 kg mol^{-1}. At low fractions of $PS_{1.5k}$-*b*-PEG_{5k}-**MAN**, the poorer surface protection from the $PEG_{1.8k}$-$\mathbf{OCH_3}$, yielding greater association, but this effect decreases as the steric layer is increased by the presence of more PEG_{5k}-**MAN** chains. At a sufficiently high fraction of $PS_{1.5k}$-*b*-PEG_{5k}-**MAN** (4%, Formulation 2.10), the particle is well protected against nonspecific association and NC association proceeds in a specific receptor mediated pathway. We find that the optimum uptake occurs at the same mannose densities for the 1.8 kg mol^{-1} and 5 kg mol^{-1} PEG coronas. Furthermore, the level of uptake for all higher mannose densities is the same ($p<0.1$) regardless of PEG corona molecular weight. To confirm that NCs are being internalized by the mannose receptor, confocal imaging was performed to determine NC localization, and blocking experiments were performed to show specificity. In Fig. 3a, for Formulation 2.4, there is a 4-fold greater extent of association at 37°C than at 4°C after 3h, and confocal sectioning shows that the majority of the NC fluorescence is in the cell cytosol (Fig. 3d). Inhibiting internalization *via* the mannose receptor with dextran, we find that a major fraction of Formulation 2.4 is internalized via MR-dependent pathway, confirming that specificity has been achieved (Fig. 4). In contrast, the association of Formulation 1.1 is unaffected, confirming that this formulation is internalized via another route, which is not specific to the mannose receptor.

MR-targeted NCs thus provide significantly increased specific uptake compared to their non-functionalized counterparts. It is important to note that this approach has been designed with non-interacting methoxy-terminated PEG to investigate the general principle of specific, optimized cell targeting, applicable to cell types other than macrophages. *In vitro* macrophage uptake is greatest when NCs are formulated with hydroxyl-terminated polymers (Fig. 4), although the hydroxyl-terminated polymers may reduce targeting specificity to macrophages *in vivo*.

5. Conclusions

The binding and internalization of targeted polymeric NCs formulated by block copolymer-directed rapid precipitation (Flash NanoPrecipitaiton) was characterized *in vitro* with macrophage-like J774, cells. The binding and uptake depends sensitively on the density of targeting mannose groups and the PEG chain providing steric stabilization of the NCs. The terminal group on PEG chains forming the NC corona is critical in determining the fate of particles: while a hydroxyl-terminated PEG chain presents a surface which associates with the cells in a size-dependent manner, a methoxy-terminated PEG chain evades recognition and, thus, presents a truly passivated surface. Mannoside-terminated PEG chains in a methoxy-terminated PEG corona increase the extent of NC binding and internalization by a mannose-receptor-specific pathway. At a density of 9% mannoside-terminated PEG chains in the corona of a methoxy-terminated PEG NC, the binding to the MR is three times higher than for the non-targeted case. Interestingly, 9% represents a maximum, and binding decreases at mannoside concentrations of 20-75%. Understanding the biological mechanisms behind this decrease in binding is of importance in designing targeted NCs. Reports of maxima in binding are only recently appearing for other cell types. This work has established that Flash NanoPrecipitation is a facile route to create libraries of surface functionalized NCs in a single step with variable ligand densities. A key advantage of this assembly process is that the step of quantifying mannose functionalization is conducted on the initial block copolymers prior to NC assembly. This is significantly easier and more

precise then attempting to post-react mannose ligands onto NCs and to quantify the concentration of the small mannose groups on the large NC construct. The role of the hydroxyl-versus methoxy-termination on the PEG, as first described by Hubbell [45], is also surprising, and the pathway for binding and internalization by macrophages is an important, unresolved question. The model we have proposed for the size-dependence of uptake is based on the number of ligands that can contact a cell surface as a function of the curvature of the NC and the density of ligands on the NC surface. The model appears to quantitatively account for the observed size dependence of NCs with a hydroxyl-terminated surface. The data showing no size dependence of uptake for the NCs with a methoxy-terminated PEG corona and the strong size dependence for the hydroxyl-terminated NCs highlights the difficulty in interpreting the literature on the size dependence of uptake when NCs with various sizes may not have exactly the same surface structure, chemistry, or functionality. This again points out the potential power of Flash NanoPrecipitation as a tool to prepare libraries to study size and targeting phenomena. Furthermore, it provides an important framework for future studies in which targeted polymeric NCs are to be formulated and evaluated to optimize delivery to specific diseased cells. In moving forward, key work includes focusing on the intracellular fate of NCs, as well as the efficacy of NC targeting *in vivo*. This platform is now being utilized to formulate novel antitubercular drugs in targeted NCs to improve co-localization of drug dose with the intracellular bacteria.

Supplementary Material

Refer to Web version on PubMed Central for supplementary material.

Acknowledgments

This work made use of the Confocal & Electron Microscopy Core Facility at Princeton University and the authors acknowledge Joe Goodhouse for expert help with confocal microscopy. This research was supported with funding from the National Science Foundation NIRT award (CBET-0506966), the National Institutes of Health (RO1 CA155061, R37 AI051214, U54AR055073 R01GM034310, R01ES004738, and P30ES005022), and the Lidlow Senior Thesis Fund.

Role of the funding sources. The sponsors played no role in the design, collection, or interpretation of the data, or writing of the manuscript.

References

[1]. WHO. Global Tuberculosis Control. World Health Organization; Geneva: 2011.

[2]. Kang PB, Azad AK, Torrelles JB, Kaufman TM, Beharka A, Tibesar E, et al. The human macrophage mannose receptor directs Mycobacterium tuberculosis lipoarabinomannan-mediated phagosome biogenesis. J. Exp. Med. 2005; 202:987–999. [PubMed: 16203868]

[3]. Fratti RA, Chua J, Vergne I, Deretic V. Mycobacterium tuberculosis glycosylated phosphatidylinositol causes phagosome maturation arrest. P. Natl. A. Sci. USA. 2003; 100:5437–5442.

[4]. Gelperina S, Kisich K, Iseman MD, Heifets L. The potential advantages of nanoparticle drug delivery systems in chemotherapy of tuberculosis. Am. J. Resp. Crit. Care. 2005; 172:1487–1490.

[5]. Azarmi S, Roa WH, Loebenberg R. Targeted delivery of nanoparticles for the treatment of lung diseases. Adv. Drug Deliver. Rev. 2008; 60:863–875.

[6]. Moghimi SM, Hunter AC, Murray JC. Long-circulating and target-specific nanoparticles: Theory to practice. Pharmacol. Rev. 2001; 53:283–318. [PubMed: 11356986]

[7]. Schlesinger LS. Macrophage phagocytosis of virulent but not attenuated strains of mycobacterium-tuberculosis is mediated by mannose receptors in addition to complement receptors. J. Immunol. 1993; 150:2920–2930. [PubMed: 8454864]

[8]. Kawakami S, Sato A, Nishikawa M, Yamashita F, Hashida M. Mannose receptor-mediated gene transfer into macrophages using novel mannosylated cationic liposomes. Gene Ther. 2000; 7:292–299. [PubMed: 10694809]

[9]. Wijagkanalan W, Kawakami S, Takenaga M, Igarashi R, Yamashita F, Hashida M. Efficient targeting to alveolar macrophages by intratracheal administration of mannosylated liposomes in rats. J. Control. Release. 2008; 125:121–130. [PubMed: 18037185]

[10]. Wijagkanalan W, Kawakami S, Yamashita F, Sasaki H, Hashida M. Targeting of dexamethasone palmitate incorporated in mannosylated liposomes to alveolar macrophages ameliorates lung inflammation in murine model. Drug Metab. Rev. 2007; 39:200–200.

[11]. Garcon N, Gregoriadis G, Taylor M, Summerfield J. Mannose-Mediated Targeted Immunoadjuvant Action of Liposomes. Immunology. 1988; 64:743–745. [PubMed: 3169846]

[12]. Johnson BK, Prud'homme RK. Chemical processing and micromixing in confined impinging jets. AIChE J. 2003; 49:2264–2282.

[13]. Reddy VM, Einck L, Nacy CA. In vitro antimycobacterial activities of capuramycin analogues. Antimicrob. Agents Ch. 2008; 52:719–721.

[14]. West NP, Cergol KM, Xue M, Randall EJ, Britton WJ, Payne RJ. Inhibitors of an essential mycobacterial cell wall lipase (Rv3802c) as tuberculosis drug leads. Chem. Commun. 2011; 47:5166–5168.

[15]. Gindy ME, Ji SX, Hoye TR, Panagiotopoulos AZ, Prud'homme RK. Preparation of Poly(ethylene glycol) Protected Nanoparticles with Variable Bioconjugate Ligand Density. Biomacromolecules. 2008; 9:2705–2711. [PubMed: 18759476]

[16]. Akbulut M, Ginart P, Gindy ME, Theriault C, Chin KH, Soboyejo W, et al. Generic Method of Preparing Multifunctional Fluorescent Nanoparticles Using Flash NanoPrecipitation. Adv. Funct. Mater. 2009; 19:718–725.

[17]. Irache JM, Salman HH, Gamazo C, Espuelas S. Mannose-targeted systems for the delivery of therapeutics. Expert Opin. Drug Del. 2008; 5:703–724.

[18]. Pontow SE, Kery V, Stahl PD. Mannose Receptor. Int. Rev. Cytol. 1992; 137B:221–244. [PubMed: 1478821]

[19]. Taylor ME, Drickamer K. Structural requirements for high-affinity binding of complex ligands by the macrophage mannose receptor. J. Biol. Chem. 1993; 268:399–404. [PubMed: 8416946]

[20]. Wileman TE, Lennartz MR, Stahl PD. Identification of the macrophage mannose receptor as a 175-kDa membrane-protein. P. Natl. A. Sci. USA. 1986; 83:2501–2505.

[21]. Copland MJ, Baird MA, Rades T, McKenzie JL, Becker B, Reck F, et al. Liposomal delivery of antigen to human dendritic cells. Vaccine. 2003; 21:883–890. [PubMed: 12547598]

[22]. Wijagkanalan W, Higuchi Y, Kawakami S, Teshima M, Sasaki H, Hashida M. Enhanced anti-inflammation of inhaled dexamethasone palmitate using mannosylated liposomes in an endotoxin-induced lung inflammation model. Mol. Pharmacol. 2008; 74:1183–1192. [PubMed: 18669445]

[23]. Mahajan S, Prashant CK, Koul V, Choudhary V, Dinda AK. Receptor Specific Macrophage Targeting by Mannose-Conjugated Gelatin Nanoparticles-An In Vitro and In Vivo Study. Current Nanoscience. 2010; 6:413–421.

[24]. Yeeprae W, Kawakami S, Yamashita F, Hashida M. Effect of mannose density on mannose receptor-mediated cellular uptake of mannosylated O/W emulsions by macrophages. J. Control. Release. 2006; 114:193–201. [PubMed: 16876282]

[25]. Wattendorf U, Coullerez G, Voros J, Textor M, Merkle HP. Mannose-based molecular patterns on stealth microspheres for receptor-specific targeting of human antigen-presenting cells. Langmuir. 2008; 24:11790–11802. [PubMed: 18785716]

[26]. Engel A, Chatterjee SK, Al-arifi A, Riemann D, Langner J, Nuhn P. Influence of spacer length on interaction of mannosylated liposomes with human phagocytic cells. Pharm. Res. 2003; 20:51–57. [PubMed: 12608536]

[27]. Fakhari A, Baoum A, Siahaan TJ, Le KB, Berkland C. Controlling Ligand Surface Density Optimizes Nanoparticle Binding to ICAM-1. J. Pharm. Sci. 2011; 100:1045–1056. [PubMed: 20922813]

[28]. Poon Z, Chen S, Engler AC, Lee HI, Atas E, von Maltzahn G, et al. Ligand-clustered "patchy" nanoparticles for modulated cellular uptake and in vivo tumor targeting. Angew. Chem. Int. Edit. 2010; 49:7266–7270.

[29]. Yamada A, Taniguchi Y, Kawano K, Honda T, Hattori Y, Maitani Y. Design of folate-linked liposomal doxorubicin to its antitumor effect in mice. Clin. Cancer Res. 2008; 14:8161–8168. [PubMed: 19088031]

[30]. Kawano K, Maitani Y. Effects of Polyethylene Glycol Spacer Length and Ligand Density on Rolate Receptor Targeting of Liposomal Doxorubicin In Vitro. J. Drug Deliv. 2010; 2011:6.

[31]. Ralph P, Nakoinz I. Phagocytosis and cytolysis by a macrophage tumor and its cloned cell line. Nature. 1975; 257:393–394. [PubMed: 1101071]

[32]. Blum JS, Stahl PD, Diaz R, Fiani ML. Purification and Characterization of the D-Mannose Receptor from J774-Mouse Macrophage Cells. Carbohyd. Res. 1991; 213:145–153.

[33]. Fiani ML, Beitz J, Turvy D, Blum JS, Stahl PD. Regulation of mannose receptor synthesis and turnover in mouse J774 macrophages. J. Leukocyte Biol. 1998; 64:85–91. [PubMed: 9665280]

[34]. Diment S, Leech MS, Stahl PD. Generation of Macrophage Variants with 5-Azacytidine - Selection for Mannose Receptor Expression. J. Leukocyte Biol. 1987; 42:485–490. [PubMed: 2445884]

[35]. Mukhopadhyay A, Stahl P. Bee venom phospholipase A(2) is recognized by the macrophage mannose receptor. Arch. Biochem. Biophys. 1995; 324:78–84. [PubMed: 7503563]

[36]. Clift MJD, Rothen-Rutishauser B, Brown DM, Duffin R, Donaldson K, Proudfoot L, et al. The impact of different nanoparticle surface chemistry and size on uptake and toxicity in a murine macrophage cell line. Toxicol. Appl. Pharm. 2008; 232:418–427.

[37]. Rehor A, Schmoekel H, Tirelli N, Hubbell JA. Functionalization of polysulfide nanoparticles and their performance as circulating carriers. Biomaterials. 2008; 29:1958–1966. [PubMed: 18242691]

[38]. Cui ZR, Hsu CH, Mumper RJ. Physical characterization and macrophage cell uptake of mannan-coated nanoparticles. Drug Development and Industrial Pharmacy. 2003; 29:689–700. [PubMed: 12889787]

[39]. Zhang SY, Adamson DH, Prud'homme RK, Link AJ. Photocrosslinking the polystyrene core of block-copolymer nanoparticles. Polym. Chem. 2011; 2:665–671.

[40]. Chan TR, Hilgraf R, Sharpless KB, Fokin VV. Polytriazoles as copper(I)-stabilizing ligands in catalysis. Org. Lett. 2004; 6:2853–2855. [PubMed: 15330631]

[41]. Aoyama T, Shioiri T. New Methods and Reagents in Organic-Synthesis .91. Trimethylsilyldiazomethane - a Convenient Reagent for the O-Methylation of Alcohols. Tetrahedron Lett. 1990; 31:5507–5508.

[42]. Liu Y, Cheng CY, Liu Y, Prud'homme RK, Fox RO. Mixing in a multi-inlet vortex mixer (MIVM) for flash nano-precipitation. Chem. Eng. Sci. 2008; 63:2829–2842.

[43]. Han J, Zhu Z, Qian H, Wohl AR, Beaman CJ, Hoye TR, et al. A Simple Confined Impingement Jets Mixer for Flash NanoPrecipitation J. Pharm. Sci. 2012

[44]. Wolak MA, Delcamp J, Landis CA, Lane PA, Anthony J, Kafafi Z. High-performance organic light-emitting diodes based on dioxolane-substituted pentacene derivatives. Adv. Funct. Mater. 2006; 16:1943–1949.

[45]. Reddy ST, van der Vlies AJ, Simeoni E, Angeli V, Randolph GJ, O'Neill CP, et al. Exploiting lymphatic transport and complement activation in nanoparticle vaccines. Nat. Biotechnol. 2007; 25:1159–1164. [PubMed: 17873867]

[46]. D'Addio SM, Saad W, Ansell SM, Squiers JJ, Adamson DH, Herrera-Alonso M, et al. Effects of block copolymer properties on nanocarrier protection from in vivo clearance. J Control Release. 2012; 162:208–217. [PubMed: 22732478]

[47]. Jeon SI, Lee JH, Andrade JD, Degennes PG. Protein Surface Interactions in the Presence of Polyethylene Oxide .1. Simplified Theory. Journal of Colloid and Interface Science. 1991; 142:149–158.

[48]. Woodle MC. Sterically Stabilized Liposome Therapeutics. Advanced Drug Delivery Reviews. 1995; 16:249–265.

[49]. Taylor ME, Bezouska K, Drickamer K. Contribution to ligand-binding by multiple carbohydrate-recognition domains in the macrophage mannose receptor. J. Biol. Chem. 1992; 267:1719–1726. [PubMed: 1730714]

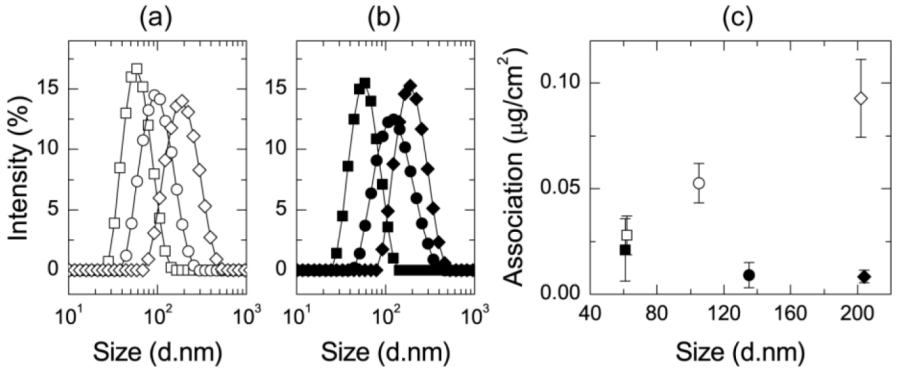

Figure 1.

The size distributions of NCs (Formulations 1.2-1.7) stabilized by (a) PS1.5k-*b*-PEG_{5k}-**OH** with an intensity average diameter of 62 nm (□), 105 nm (○), and 202 nm (◇) and (b) $PLA_{3.8k}$-b-PEG_{5k}-$\mathbf{OCH_3}$ with an intensity average diameter of 61 nm (■), 135 nm (●), and 204 nm (◆). (c) After incubation with J774A.1 cells at 4°C, there is low association with $PLA_{3.8k}$-*b*-PEG_{5k}-$\mathbf{OCH_3}$ stabilized particles. Association increases with particle size for $PS_{1.5k}$-*b*-PEG_{5k}-**OH** stabilized formulations.

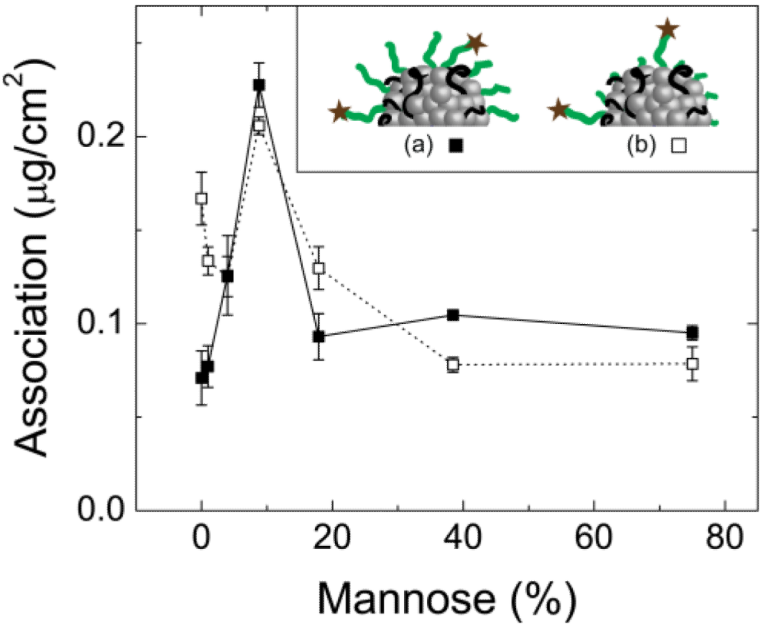

Figure 2.

Extent of NC association as a function of the percent of $PS_{1.5k}$-*b*-PEG_{5k}-**MAN** chains relative to PS_{m}-*b*-PEG_{n}-$\mathbf{OCH_3}$ on the NC surface formulations in Table 2). The methoxy-terminated stabilizer was (■) $PS_{1.5k}$-*b*-PEG_{5k}-$\mathbf{OCH_3}$ or (□) $PS_{1.6k}$-*b*-$PEG_{1.8k}$-$\mathbf{OCH_3}$. The dose was 100 μg mL^{-1}. Inset: Schematic of the relative PEG block lengths, where (a) both methoxy- and mannoside-terminated PEG chains were 5 kg mol^{-1} or (b) the methoxy-terminated PEG chains were 1.8 kg mol^{-1} and the mannose-terminated PEG chains were 5 kg mol^{-1}.

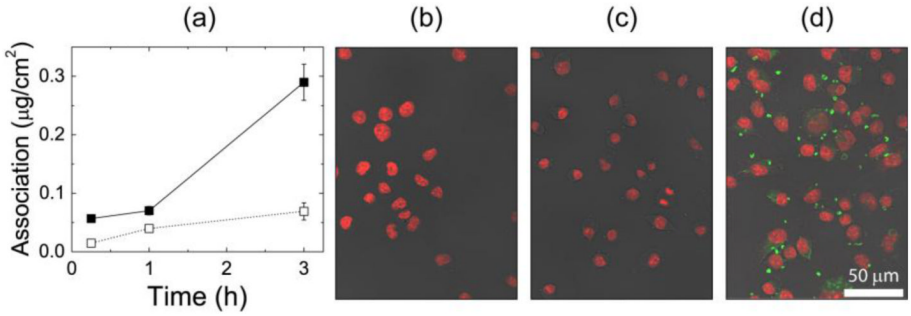

Figure 3.

Association of NC with 9% surface mannoside (Formulation 2.4). (a) Time and temperature dependence of cellular association with J774E cells as a function of time at 4°C (□) and 37°C (■). Extent of association was quantified by cell lysis and solubilization of the hydrophobic dye. (b-d) Representative confocal images of fixed J774E cells, corresponding to the following conditions: (b) cells not exposed to NCs (c) cells exposed to NCs for 3 h at 4°C, and (d) cells exposed to NCs for 3 h at 37°C. The DAPI nuclear stain is shown in red and EtTP5 fluorescence is shown in green.

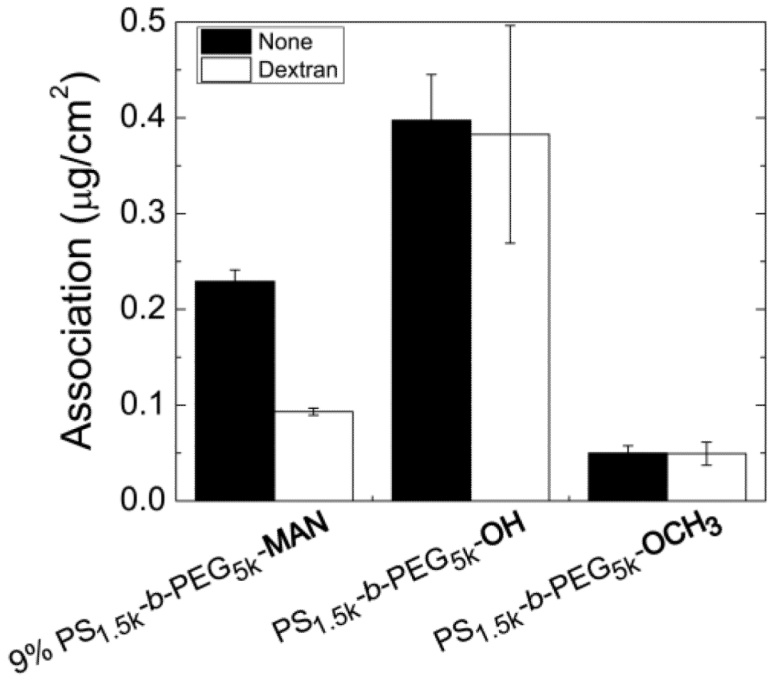

Figure 4.
Quantified NC association at 37°C in J774E cells without a blocking ligand (black bars) and with dextran to block binding to the mannose receptor (white bars). All NCs are dosed at 100 μg mL^{-1}.

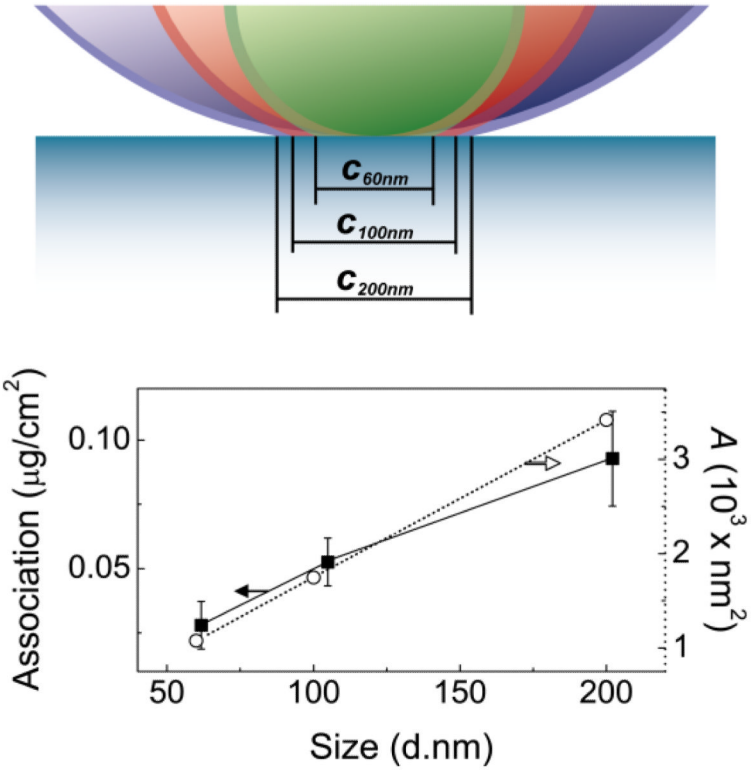

Figure 5.

Contact area between a NC with a diameter of 60, 100, or 200 nm at a separation distance of 5.3 nm, which corresponds to the radius of gyration for 5 kg mol^{-1} PEG (figure drawn to scale). The chord length, c_i, in the image corresponds to the diameter of the contact area, A. The calculated contact area (○) varies linearly with the particle diameter, d, and is proportional to the mass of Formulations 1.2-1.5 associated with J774A.1 cells at 4 °C (■).

Table 1

THF solution composition for NC assembly in FNP.

Formulation	stabilizer		core			NC diameter (nm)
	block copolymer	c_{bcp} [a] (mg mL^{-1})	filler	c_{filler} [b] (mg mL^{-1})	c_{EtTP5} [c] (mg mL^{-1})	
1.1	$PS_{1.5k}$-*b*-PEG_{5k}-**OH**	10	$PS_{1.5k}$-OH	7.5	2.5	115
1.2	$PS_{1.5k}$-*b*-PEG_{5k}-**OH**	10	VE	5	0.25	62
1.3	$PS_{1.5k}$-*b*-PEG_{5k}-**OH**	10	VE	12	0.6	105
1.4	$PS_{1.5k}$-*b*-PEG_{5k}-**OH**	10	VE	22	1.1	202
1.5	$PLA_{3.8k}$-*b*-PEG_{5k}-**OCH_3**	20	VE	6	0.3	61
1.6	$PLA_{3.8k}$-*b*-PEG_{5k}-**OCH_3**	20	VE	20	1	135
1.7	$PLA_{3.8k}$-*b*-PEG_{5k}-**OCH_3**	20	VE	40	2	204

[a] cBCP is the concentration of block copolymer in THF

[b] c_{filler} is the concentration of filler (either $PS_{1.5k}$-OH or VE) in THF

[c] c_{EtTP5} is the concentration of EtTP5 in THF

Table 2

Compositions of the THF solutions used for precipitation of MR-targeted NC formulations

Formulation	mannose endgroups (%)	passive stabilizer PEG M*w*, *n*[a] (kg mol^{-1})	stabilizers		Core		NC diameter (nm)
			PS_m-*b*-PEG_n-OCH_3 (mg mL^{-1})	$PS_{1.5k}$-*b*-PEG_{5k}-MAN (mg mL^{-1})	c_{filler}[b] (mg mL^{-1})	c_{EtTP5}[c] (mg mL^{-1})	
2.1	0	5	9.5	0	7.1	2.4	180
2.2	1	5	9.4	0.1	7.1	2.4	220
2.3	4	5	9.1	0.4	7.1	2.4	120
2.4	9	5	8.7	0.8	7.1	2.4	130
2.5	18	5	7.8	1.7	7.1	2.4	80
2.6	38	5	5.8	3.6	7.1	2.4	130
2.7	75	5	2.3	7.2	7.1	2.4	80
2.8	0	1.8	5	0	7.1	2.4	120
2.9	1	1.8	4.9	0.1	7.1	2.4	80
2.1	4	1.8	4.8	0.4	7.1	2.4	130
2.11	9	1.8	4.5	0.8	7.1	2.4	120
2.12	18	1.8	4.1	1.7	7.1	2.4	120
2.13	38	1.8	3.1	3.6	7.1	2.4	70
2.14	75	1.8	1.2	7.2	7.1	2.4	80

[a] The passive stabilizer is the methoxy-terminated PS_{m}-*b*-PEG_{n}-**OCH_3** polymer used in the formulation, and *n* is the M*w* of the PEG block

[b] c_{filler} is the concentration of $PS_{1.5k}$-OH in THF

[c] c_{EtTP5} is the concentration of EtTP5 in THF